

Effects of solid fission products forming dissolved oxide (Nd) and metallic precipitate (Ru) on the thermal conductivity of uranium base oxide fuel

Dong-Joo Kim*, Jae-Ho Yang, Jong-Hun Kim, Young-Woo Rhee,
Ki-Won Kang, Keon-Sik Kim, Kun-Woo Song

Korea Atomic Energy Research Institute, P.O. Box 150, Yuseong, Daejeon 305-353, South Korea

Available online 9 December 2006

Abstract

The effects of solid fission products on the thermal conductivity of uranium base oxide nuclear fuel were experimentally investigated. Neodymium (Nd) and ruthenium (Ru) were added to represent the physical states of solid fission products such as ‘dissolved oxide’ and ‘metallic precipitate’, respectively. Thermal conductivity was determined on the basis of the thermal diffusivity, density and specific heat values. The effects of the additives on the thermal conductivity were quantified in the form of the thermal resistivity equation – the reciprocal of the phonon conduction equation – which was determined from the measured data. It is concluded that the thermal conductivity of the irradiated nuclear fuel is affected by both the ‘dissolved oxide’ and the ‘metallic precipitate’, however, the effects are in the opposite direction and the ‘dissolved oxide’ influences the thermal conductivity more significantly than that of the ‘metallic precipitate’.

© 2006 Elsevier B.V. All rights reserved.

Keywords: Thermal conductivity; Solid fission product; Uranium oxide

1. Introduction

Uranium dioxide (UO₂) has been typically used as a nuclear fuel material for the light water reactor (LWR). LWR is currently the most prevalent reactor type used for a power production. The thermal conductivity of nuclear fuel materials is one of the most important properties for evaluating a fuel performance in a nuclear reactor, because this property affects the fuel centerline temperature, operating power efficiency, safety, release of the fission product, etc. For example, a decrement of the thermal conductivity reduces the efficiency of the operating power, and increases the fuel centerline temperature. And the increment of the fuel temperature can affect a release of the fission products. There are several factors that decrease the thermal conductivity of oxide fuel materials in a nuclear reactor: (a) fission products forming a solid solution, (b) a perturbation of the stoichiometry for the fuel element, (c) an increasing reactor burnup, etc. Unfortunately, under reactor operating conditions, a decrease of the thermal conductivity is unavoidable. To minimize the decrease of the thermal conductivity of fuel materials, the thermal con-

ductivities of UO₂ and various elements added-UO₂ (Gd, Dy, Cr, etc.) have been widely studied by many investigators [1–10].

In a nuclear reactor, the fission products have several kinds of physical or chemical states [11]. The states of numerous fission products have been classified into four groups [11–13]: (a) fission products dissolved as oxides in the fuel matrix, (b) fission products forming metallic precipitates, (c) fission products forming oxide precipitates and (d) fission gases and other volatile fission products. This classification can be applied to the case of a uranium base oxide fuel as well as a UO₂ fuel.

It was intended to show the effects of the physical states of solid fission products on the thermal conductivity of UO₂ and (U_{0.924}Ce_{0.076})O₂. (U_{0.924}Ce_{0.076})O₂ is a simulated composition of a light water reactor-mixed oxide (LWR-MOX) fuel. Usually, cerium oxide has been used as a simulating material for plutonium oxide, owing to its similar chemical/thermodynamic behaviors and a convenience in handling [14–16], even though cerium oxide cannot duplicate the behaviors of plutonium oxide exactly.

In the present work, the thermal diffusivities and linear thermal expansions of the UO₂ and (U_{0.924}Ce_{0.076})O₂ pellets were measured. The pellets contain Nd or Ru as a simulated fission product. The thermal conductivities were determined using the density, the thermal diffusivity and the specific heat data. Nd

* Corresponding author. Tel.: +82 42 868 2816; fax: +82 42 861 7340.
E-mail address: djkim@kaeri.re.kr (D.-J. Kim).

and Ru represented the physical state of a solid fission product, a dissolved oxide and a metallic precipitate, respectively. On the basis of the experimental results, it was intended to explain a thermal conductivity degradation of a uranium base oxide fuel.

2. Experimental

Various contents of Nd_2O_3 (Aldrich, 99.9%) or RuO_2 (Aldrich, 99.9%) powders were added to UO_2 (BNFL, IDR- UO_2) and CeO_2 (Aldrich, 99.9%), and then mixed for 1 h using a Turbula™ mixer. The powder mixtures were milled for 4 h using an attrition mill. Green pellets were formed by pressing the milled powder mixture at about 300 MPa, and then sintered at 2023 K for 4 h in a flowing H_2 atmosphere [17]. The size of the sintered pellets was about 8.5 mm in diameter and 12–13 mm in height.

For the purpose of analyzing the physical state of the additives in the pellets, the lattice parameters and theoretical densities were calculated using the peaks, which were measured by X-ray diffraction (XRD, Mac Science, MAC-M03XHF) from $2\theta = 10^\circ$ to 120° at room temperature using a $\text{Cu K}\alpha$ target. The step scanning method was used (counting time = 5 s, step width = 0.05°).

As a function of temperature, an axial length change of the pellets was measured in the temperature range between room temperature and 1673 K under a flowing argon atmosphere using a thermo-mechanical analyzer (TMA, SETARAM, TMA92), and the heating rate of 5 K/min was applied, according to the ASTM Designation [18]. The density was calculated using the measured thermal expansion data.

Samples for the thermal diffusivity measurement were cut to 0.9–1.1 mm in thickness and 6 mm in diameter from a sintered pellet and polished. In the temperature range of 298–1673 K, the thermal diffusivity was measured using a laser flash apparatus (LFA, Netzsch, LFA-427). The measurements of the thermal diffusivity were carried out three times at every test temperature step in a vacuum (10^{-4} – 10^{-5} Pa). The thermal conductivities were calculated from the density, the thermal diffusivity and the specific heat. Data from a literature survey [19–24] were used to calculate the specific heat through the Neumann–Kopp's law.

3. Results and discussion

3.1. Analysis of the XRD peak pattern

Fig. 1 shows the XRD patterns of the $(\text{U}, \text{Ce}, \text{Nd})\text{O}_2$ (the ratio of U/Ce is fixed according to $(\text{U}_{0.924}\text{Ce}_{0.076})\text{O}_2$, $0 \leq [\text{Nd}] \leq 0.133$ mole fraction) with several Nd contents. The $(\text{U}_{0.924}\text{Ce}_{0.076})\text{O}_2$ peaks tend to be retained, with the measured peaks being gradually shifted to the right-hand side with increasing Nd contents. That is to say, the crystal structure (fluorite structure) of UO_2 can remain, regardless of the addition of Nd or Ce. In the reaction of UO_2 , CeO_2 and Nd_2O_3 , it was confirmed that the CeO_2 and Nd_2O_3 in the UO_2 matrix was fully formed as a solid solution in this composition range. In the same manner, the XRD peaks of $(\text{U}_{0.924}\text{Ce}_{0.076})\text{O}_2 + \text{Ru}$ ($0 \leq [\text{Ru}] \leq 0.07$ mole fraction) were measured and analyzed (Fig. 2). In the case of Ru in $(\text{U}, \text{Ce})\text{O}_2$, although RuO_2 powder instead of Ru was

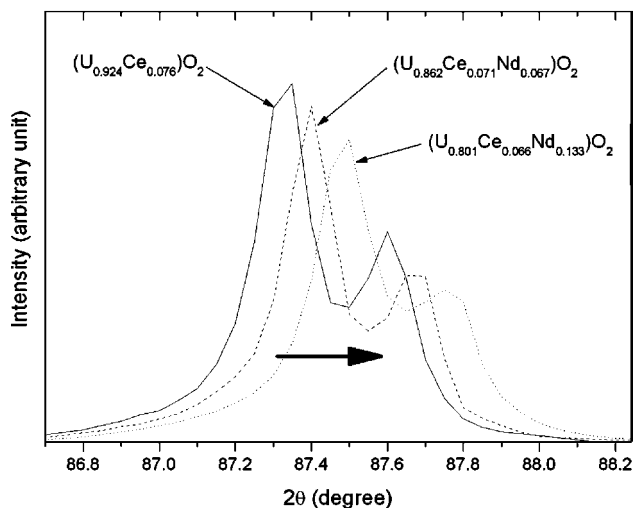


Fig. 1. XRD pattern of the $(\text{U}, \text{Ce}, \text{Nd})\text{O}_2$ samples with several Nd contents.

used, it was shown that the Ru in the UO_2 matrix existed as a metallic precipitate, because the decomposition temperature of RuO_2 (1473 K) is lower than the sintering temperature (2023 K) of this experiment, and the oxygen potential of RuO_2 is much higher than that of UO_2 and CeO_2 , i.e. ruthenium can exist as a metallic precipitate. Therefore, the peak of the Ru gradually rises with an increasing Ru content.

The calculated lattice parameters from the measured peak data are shown in Fig. 3, and the results for $(\text{U}_{0.924}\text{Ce}_{0.076})\text{O}_2$ were in good agreement with the reference data [14–16]. The lattice parameter was calculated by using a Nelson–Riley method [25] from the XPRESS™ program (X-ray powder research software). Table 1 shows the fitting parameters for the relationship ($a = a_1 + a_2x$) between the lattice parameter a in nm and the additive content (x , mole fraction).

The lattice parameter of $(\text{U}, \text{Ce}, \text{Nd})\text{O}_2$ in Fig. 3 decreases with an increasing Nd content, i.e. the data follow Vegard's law. In the case of $(\text{U}, \text{Ce})\text{O}_2 + \text{Ru}$, on the other hand, the difference of

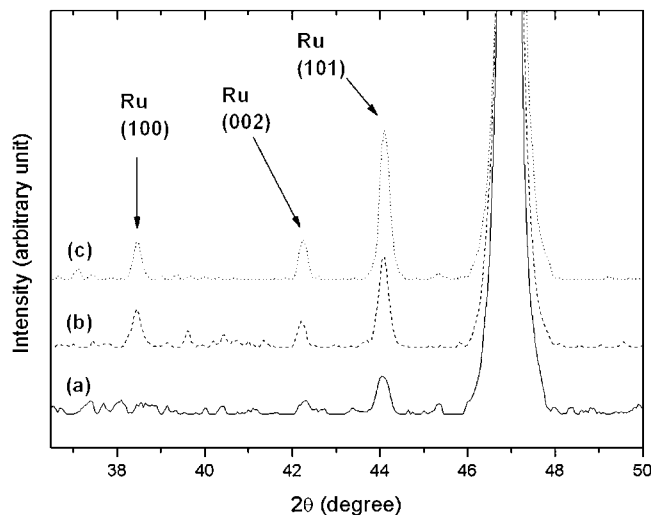


Fig. 2. XRD pattern of the $(\text{U}, \text{Ce})\text{O}_2 + \text{Ru}$ samples with several Ru content (mole fraction): (a) 0.02, (b) 0.05 and (c) 0.07.

Table 1

The fitting parameters of the lattice parameter (nm) for all the samples as a function of the additive content (x)

	(U, Ce)O ₂ ($0 \leq [\text{Ce}] \leq 0.3$)	(U, Ce, Nd)O ₂ ^a ($0 \leq [\text{Nd}] \leq 0.133$)	(U, Ce)O ₂ + Ru ^a ($0 \leq [\text{Ru}] \leq 0.07$)
a_1	0.54697(2) ^b	0.54651(5)	0.54652(2)
a_2	-0.00582(4)	-0.0062(7)	-0.00072(5)

^a The unit of additive contents is mole fraction. And it was ultimately intended to observe the effect of additive on the (U, Ce)O₂ system. So, in the ternary composition, the ratio of U/Ce was fixed according to (U_{0.924}Ce_{0.076})O₂.

^b The figure in the parenthesis is an estimated standard deviation.

lattice parameter was very small. It is suggested that the metallic precipitate hardly affected the crystal structure of the base material. The theoretical densities can be easily calculated by using the data of lattice parameter, because the fluorite structure is not changed.

The oxygen-to-metal (O/M) ratio of these samples is likely to be stoichiometric or near-stoichiometric. Even if oxygen vacancies were formed at a high temperature, an oxygen pick-up from air during storage could fill the oxygen vacancies, because a solid solution containing an oxygen deficiency is very susceptible to oxidation [26]. Many investigators [27–30] have reported that hypo-stoichiometric (U, Ln)O_{2-x} has been oxidized easily in air, even at room temperature, to almost a stoichiometric composition. Thus, although the samples in this work were sintered in a H₂ atmosphere, the O/M ratio actually remains a near-stoichiometric state (2.00–1.99). That is to say, the effect of stoichiometry on the thermal conductivity is negligible.

3.2. The thermal conductivity calculations from the density, the thermal diffusivity and the specific heat

The linear thermal expansion was measured using TMA, and then, the measured data were fitted as a function of the temperature using a cubic polynomial regression ($\Delta L/L(\%) = a + bT + cT^2 + dT^3$), and the fitting parameters are given in Table 2, where T is the absolute temperature (K) and T_0 , the initial temperature, is 298 K.

From the data of the measured length change and the following relationship [31], the density change as a function of the temperature was obtained, and it was fitted using a cubic

polynomial regression (Table 3).

$$\frac{\Delta\rho}{\rho_0} = \frac{1 - (1 + \Delta L/L_0)^3}{(1 + \Delta L/L_0)^3} \quad (1)$$

where $\Delta\rho$ is the density change, ρ_0 the initial density, ΔL the length change and L_0 is the initial length of a sample pellet. The thermal conductivity was calculated using the equation of $k = \alpha_M c_p \rho_M$. The thermal diffusivity, α_M , was measured using the laser flash method. The density, ρ_M , was calculated from the measured linear expansion data. The specific heat, c_p , was calculated from a literature data [19–24] for individual component materials using Neumann–Kopp’s law. For a comparison of the different compositions, all the thermal conductivities were normalized to the 95% theoretical density using the modified Loeb equation [32], $k_M = k_{th}(1 - P\eta)$, where k_{th} is the thermal conductivity of a fully dense material, k_M the thermal conductivity of a sample with a density of ρ_M , P the porosity, η the experimental parameter expressed as $2.6\text{--}5 \times 10^{-4}T$ [31] and T is the temperature for the measurements, in Kelvin.

3.3. Effects of solid fission products on the thermal conductivity of a uranium base oxide fuel

For a ‘dissolved oxide’ sample in the (U, Ce)O₂ matrix, Fig. 4 shows gradually decreasing thermal conductivities of (U, Ce, Nd)O₂ with an increasing Nd content. The thermal conductivity data were fitted using the phonon conduction equation $k = (A + BT)^{-1}$, because it is sufficiently enough to describe a

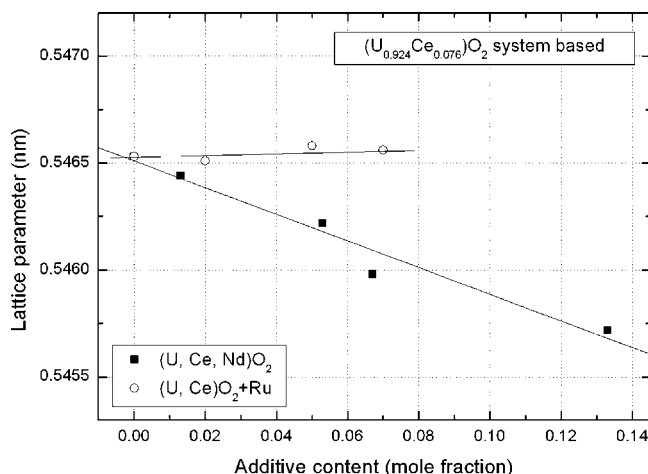


Fig. 3. The calculated lattice parameters of (U, Ce)O₂ + additive (Nd₂O₃ or Ru) as a function of the additive contents.

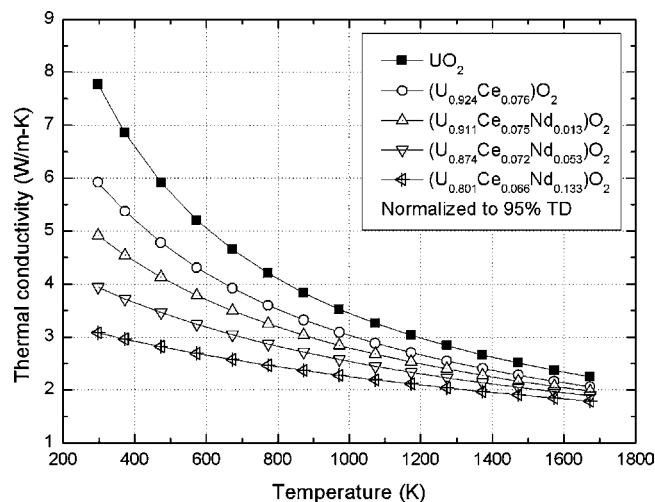


Fig. 4. Thermal conductivities of (U, Ce, Nd)O₂ with varied Nd contents as a function of the temperature.

Table 2

The fitting parameters of the linear thermal expansion (%) for all the samples as a function of the temperature ($100\Delta L/L_0 = a + bT + cT^2 + dT^3$), 293–1673 K

Composition	a	b ($\times 10^{-3}$, K^{-1})	c ($\times 10^{-7}$, K^{-2})	d ($\times 10^{-11}$, K^{-3})
UO ₂	−0.3042(9)	0.977(3)	−0.42(3)	6.35(9)
(U _{0.924} Ce _{0.076})O ₂	−0.3260(9)	1.090(4)	−0.46(4)	4.9(1)
(U _{0.911} Ce _{0.075} Nd _{0.013})O ₂	−0.329(1)	1.050(4)	−0.1(5)	4.2(2)
(U _{0.874} Ce _{0.072} Nd _{0.053})O ₂	−0.3100(1)	1.030(3)	0.45(3)	1.9(1)
(U _{0.801} Ce _{0.066} Nd _{0.133})O ₂	−0.2934(7)	0.968(3)	1.16(3)	0.59(9)
(U _{0.924} Ce _{0.076})O ₂ + 2 mol% Ru	−0.296(2)	0.943(6)	0.96(7)	0.6(2)
(U _{0.924} Ce _{0.076})O ₂ + 5 mol% Ru	−0.3203(8)	1.040(3)	0.47(4)	0.6(1)
(U _{0.924} Ce _{0.076})O ₂ + 7 mol% Ru	−0.3291(8)	1.080(3)	0.22(3)	1.3(1)

Table 3

The fitting parameters of the density (ρ in g/cm^3) for all the samples as a function of the temperature ($\rho = a + bT + cT^2 + dT^3$), 293–1673 K

Composition	a	b ($\times 10^{-4}$, K^{-1})	c ($\times 10^{-8}$, K^{-2})	d ($\times 10^{-11}$, K^{-3})
UO ₂	11.0497(3)	−3.21(1)	1.5(1)	−1.81(3)
(U _{0.924} Ce _{0.076})O ₂	10.7876(3)	−3.51(1)	1.8(1)	−1.39(4)
(U _{0.911} Ce _{0.075} Nd _{0.013})O ₂	10.7197(4)	−3.36(1)	0.6(2)	−1.11(5)
(U _{0.874} Ce _{0.072} Nd _{0.053})O ₂	10.5076(2)	−3.204(9)	−1.2(1)	−0.35(3)
(U _{0.801} Ce _{0.066} Nd _{0.133})O ₂	10.0905(2)	−2.935(8)	−3.02(9)	−0.0026(3)
(U _{0.924} Ce _{0.076})O ₂ + 2 mol% Ru	10.7954(5)	−3.05(2)	−2.7(2)	−0.024(7)
(U _{0.924} Ce _{0.076})O ₂ + 5 mol% Ru	10.8297(3)	−3.39(1)	−0.9(1)	−0.09(4)
(U _{0.924} Ce _{0.076})O ₂ + 7 mol% Ru	10.8506(3)	−3.51(1)	−0.1(1)	−0.33(4)

thermal conductivity using the lattice contribution only, in the temperature region of this experiment (from room temperature to 1673 K). The fitted values of the coefficients A and B for each sample are shown in Table 4.

Through a thermal resistivity equation – the reciprocal of the phonon conduction equation – the effects of additives on the thermal conductivity of the samples were quantified.

$$w = \frac{1}{k} = w_l + w_p = A + BT, \quad (2)$$

$$A = A_0 + \Delta A, \quad B = B_0 + \Delta B, \quad (3)$$

where w is the thermal resistivity, w_l the lattice defect thermal resistivity (A), w_p the intrinsic thermal resistivity (BT), A_0 and B_0 the coefficients for UO₂ and ΔA and ΔB are the perturbations of the coefficient.

In Fig. 5(a), it is shown that the lattice defect thermal resistivity increases with an increasing Nd content. Because the O/M ratio of the samples is a near-stoichiometric state, it can be

suggested that the Nd content is primarily responsible for the change of the thermal conductivity of (U, Ce, Nd)O₂. It is mainly attributable to the increasing lattice defect thermal resistivity caused by the U⁴⁺, Ce⁴⁺, Nd³⁺ and O^{2−} ions as point defects, i.e. phonon scattering centers. The mean free path of phonon can be decreased in the presence of point defects in a solid. Also, the mass difference between the host (U) and the substituted atom (Nd or Ce) can be suggested to be point defects which interrupt a transport of the heat energy.

Fig. 5(b) shows that the intrinsic thermal resistivity decreases with an increasing Nd content, however, the magnitude of perturbation of coefficient B is very small. The phonon–phonon scattering (the intrinsic thermal resistivity) is due to the anharmonic components of the crystal vibrations, i.e. lattice anharmonicity increases with the mass difference between the anions and cations in an ionic material [33]. But, in this work, the mass difference between the host (U⁴⁺) and the substituted cation (Ce⁴⁺ or Nd³⁺) is very large, so the influence between Nd³⁺ and O^{2−} can be regarded as relatively small.

On the other hand, it was shown that the thermal conductivities of the ‘metallic precipitate’ sample increased with increasing Ru-metal contents (Fig. 6). This result can be readily expected from the fact that the thermal conductivity of a metal is intrinsically high compared with that of a ceramic material. In a metal, it is well known that free electrons effectively transport the thermal energy instead of the phonon in a ceramic. Fig. 7 shows that the lattice defect thermal resistivity decreases and that the intrinsic thermal resistivity is hardly perturbed with an increasing Ru content. That is to say, the transportation of thermal energy through Ru-metal results in a lower thermal resistivity. Consequently, the thermal conductivity of (U, Ce)O₂ + Ru increased.

Table 4

Calculated values of A and B of a sample from the fitting relationship, 293–1673 K

Composition	A (m K/W)	B (m/W)
UO ₂	0.060(1)	0.000230(2)
(U _{0.924} Ce _{0.076})O ₂	0.100(3)	0.000230(5)
(U _{0.911} Ce _{0.075} Nd _{0.013})O ₂	0.138(5)	0.000220(7)
(U _{0.874} Ce _{0.072} Nd _{0.053})O ₂	0.194(4)	0.000200(5)
(U _{0.801} Ce _{0.066} Nd _{0.133})O ₂	0.274(4)	0.000170(5)
(U _{0.924} Ce _{0.076})O ₂ + 2 mol% Ru	0.087(3)	0.000240(5)
(U _{0.924} Ce _{0.076})O ₂ + 5 mol% Ru	0.081(7)	0.00024(1)
(U _{0.924} Ce _{0.076})O ₂ + 7 mol% Ru	0.072(2)	0.000250(4)

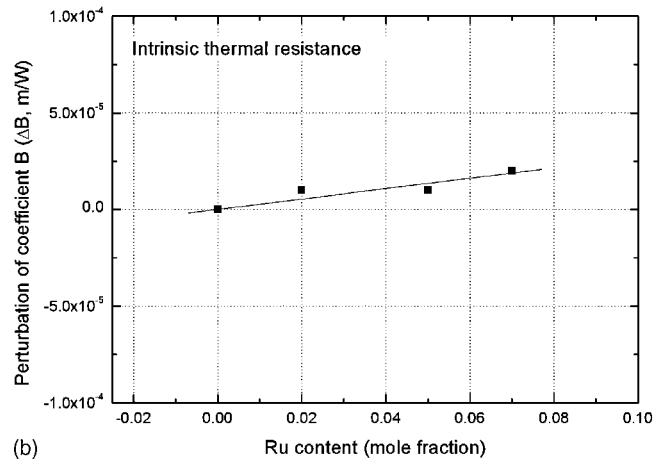
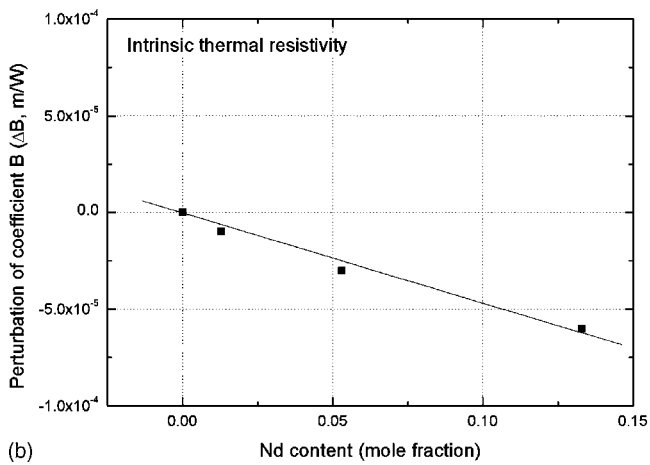
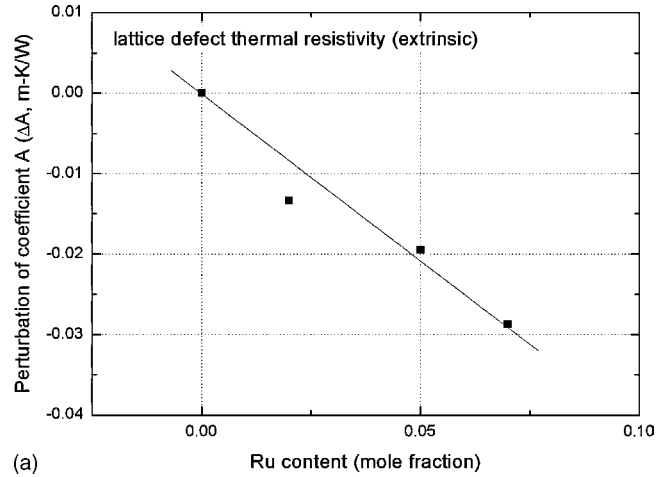
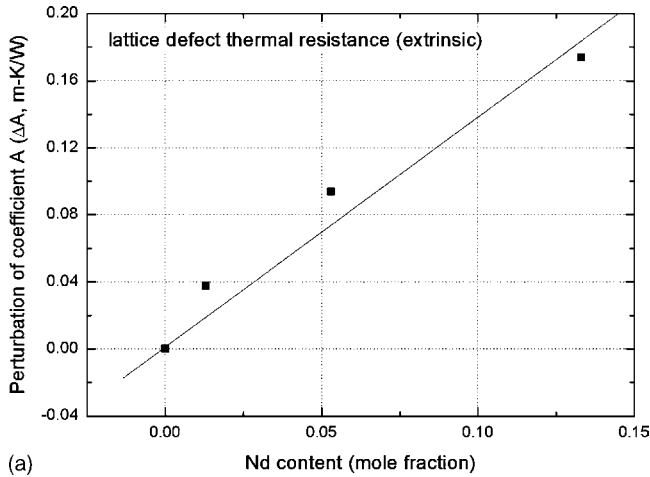


Fig. 5. Relationship between the perturbation of the fitted coefficients and the Nd content in the (U, Ce, Nd)O₂: (a) lattice defect thermal resistivity and (b) intrinsic thermal resistivity.

Fig. 7. Relationship between the perturbation of the fitted coefficients and the Ru content in the (U, Ce)O₂ + Ru: (a) lattice defect thermal resistivity and (b) intrinsic thermal resistivity.

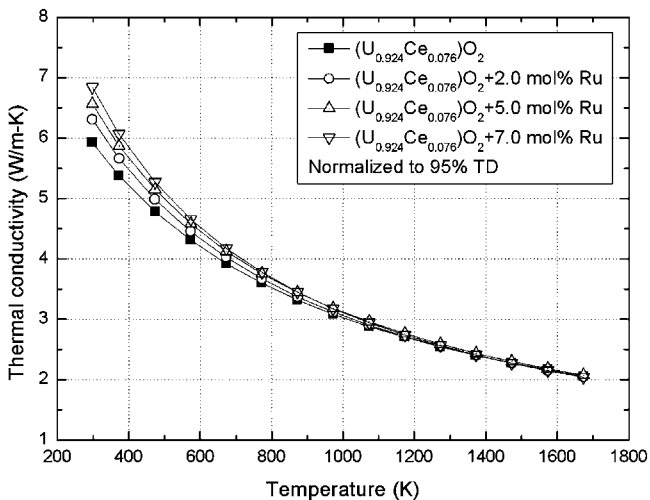


Fig. 6. Thermal conductivities of (U, Ce)O₂ + Ru with varied Ru contents as a function of the temperature.

The thermal conductivities of the ‘metallic precipitate’ sample obviously increased, however, the magnitude of their increment was not large, because the metal elements (Ru) were isolated as a form of a precipitate. If the metal elements are continuously connected along the grain boundary, it may show the effect of a large increment on the thermal conductivity.

From the measured data in this study, the relationship between the thermal conductivity (k) and the content of an additive (y) as a function of the temperature was derived in the following way, and the coefficients of A_1 , A_2 , B_1 and B_2 are shown in Table 5.

$$k = \frac{1}{(A_1 + A_2y) + (B_1 + B_2y)T} \quad (4)$$

where A and B are the phonon–lattice defect interaction and the phonon–phonon interaction, 1 and 2 are y -independent and y -dependent term, respectively.

The thermal conductivity of the irradiated nuclear fuel which contains fission products might be affected by both the ‘dissolved oxide’ and the ‘metallic precipitate’. The former degrades the thermal conductivity of a fuel significantly, and the latter increases it, only slightly. Therefore, the thermal conductivity

Table 5

Relationship between the thermal conductivity and the content of the additive as a function of the temperature—the coefficients of A_1 , A_2 , B_1 , and B_2 , 293–1673 K

	(U, Ce, Nd)O ₂ (0 ≤ [Nd] ≤ 0.133) ^a	(U, Ce)O ₂ + Ru (0 ≤ [Ru] ≤ 0.07)
A_1 (m K/W)	0.100(3)	0.100(3)
A_2 (m K/W)	1.4(1)	−0.42(3)
B_1 (m/W)	0.000230(5)	0.000230(5)
B_2 (m/W)	0.00047(3)	0.00027(4)

^a The unit of additive contents is mole fraction.

of the irradiated fuel decreases with an increasing content of the solid fission product.

4. Conclusions

This study experimentally investigated the effects of solid fission products on the thermal conductivities of a uranium base oxide fuel. Nd and Ru were selected for the experiments to represent the physical states of the solid fission product as a ‘dissolved oxide’ and a ‘metallic precipitate’, respectively.

- (1) For the ‘dissolved oxide’ sample in the UO₂ matrix, the thermal conductivity decreased with an increasing Nd content. This effect is mainly attributed to the increase in the lattice point defects which play the role of phonon scattering centers, that is, a mean free path of a phonon scattering decreases with increasing the point defects, thus it increases the thermal resistivity.
- (2) For the ‘metallic precipitate’ sample, the thermal conductivity increased slightly with increasing Ru-metal contents, because the transportation of thermal energy through metallic precipitate results in a lower thermal resistivity.
- (3) The degrading effect of a dissolved oxide on the thermal conductivity is larger than the enhancing effect of metallic precipitates, so the thermal conductivity of the uranium oxide fuel decreases with an increasing content of the solid fission products.

Acknowledgement

The authors acknowledge that this work has been performed under the Nuclear Mid- and Long-term R&D Projects supported by the Ministry of Science and Technology in Korea.

References

- [1] D.G. Martin, *J. Nucl. Mater.* 110 (1982) 78.
- [2] M. Hirai, S. Ishimoto, *J. Nucl. Sci. Technol.* 28 (11) (1991) 995.
- [3] M.V. Krishnaiah, G. Seenivasan, P. Murti, C.K. Mathews, *J. Nucl. Mater.* 306 (2002) 10.
- [4] R. Gibby, BNWL-927, Battelle Northwest, Richland, Wash. Pacific Northwest Lab., 1969.
- [5] R. Gibby, *J. Nucl. Mater.* 38 (1971) 163.
- [6] S. Fukushima, T. Ohmichi, A. Maeda, H. Watanabe, *J. Nucl. Mater.* 102 (1981) 30.
- [7] S. Fukushima, T. Ohmichi, A. Maeda, H. Watanabe, *J. Nucl. Mater.* 105 (1982) 201.
- [8] G.J. Hyland, *J. Nucl. Mater.* 113 (1983) 125.
- [9] S. Fukushima, T. Ohmichi, A. Maeda, M. Handa, *J. Nucl. Mater.* 114 (1983) 312.
- [10] H.J. Lee, C.W. Kim, *J. Korean Nucl. Soc.* 8 (2) (1976) 81.
- [11] H. Kleykamp, *J. Nucl. Mater.* 131 (1985) 221.
- [12] P.G. Lucuta, R.A. Verrall, H. Matzke, B.J. Palmer, *J. Nucl. Mater.* 178 (1991) 48.
- [13] J. Cobos, D. Papaioannou, J. Spino, M. Coquerelle, *J. Alloys Compd.* 271–273 (1998) 610.
- [14] D.I.R. Norris, P. Kay, *J. Nucl. Mater.* 116 (1983) 184.
- [15] K. Yamada, S. Yamanaka, T. Nakagawa, M. Uno, M. Katsura, *J. Nucl. Mater.* 247 (1997) 289.
- [16] K. Nagarajan, R. Saha, R.B. Yadav, S. Rajagopalan, K.V.G. Kutty, M. Saibaba, P.R. Vasudeva Rao, C.K. Mathews, *J. Nucl. Mater.* 130 (1985) 242.
- [17] D.J. Kim, Y.W. Lee, Y.S. Kim, *J. Nucl. Mater.* 342 (2005) 192.
- [18] ASTM Designation, E831-03.
- [19] Outokumpu HSC chemistry 4.0 for windows, Chemical reaction and equilibrium software with extensive thermochemical database, 1999.
- [20] E.H.P. Cordfunke, R.J.M. Konings, *Thermochemical Data for Reactor Materials and Fission Products*, North Holland, Amsterdam, 1990.
- [21] D.L. Hagrman, G.A. Reymann, R.E. Mason, NUREG/CR-0479 TREE-1280, Rev.2 (1981) 1–529.
- [22] J.K. Fink, *J. Nucl. Mater.* 279 (2000) 1.
- [23] J.J. Carbajo, G.L. Yoder, S.G. Popov, V.K. Ivanov, *J. Nucl. Mater.* 299 (2001) 181.
- [24] Y. Arita, T. Matsui, S. Hamada, *Thermochim. Acta* 253 (1995) 1.
- [25] J.B. Nelson, D.P. Riley, *Proc. Phys. Soc.* 57 (1945) 160.
- [26] T. Ohmichi, S. Fukushima, A. Maeda, H. Watanabe, *J. Nucl. Mater.* 102 (1981) 40.
- [27] R.J. Beals, J.H. Handwerk, *J. Am. Ceram. Soc.* 48 (5) (1965) 271.
- [28] J.F. Wadier, CEA-R-4507, Fontenay (1973).
- [29] K. Une, M. Oguma, *J. Nucl. Mater.* 110 (1982) 215.
- [30] H. Tagawa, T. Fujino, *J. At. Energy Soc. Jpn.* 22 (1980) 871.
- [31] J.K. Fink, <http://www.insc.anl.gov/matprop/>, MATPRO (1999).
- [32] A.L. Loeb, *J. Am. Ceram. Soc.* 37 (1954) 96.
- [33] D.R. Olander, *Fundamental aspects of nuclear reactor fuel elements*, TID-26711-P1 (1976) 122.